Synthesis of GaN_xAs_{1-x} Thin Films by Pulsed Laser Melting and Rapid Thermal Annealing (PLM-RTA) of N^+-implanted GaAs

K. M. Yu, W. Walukiewicz,
Materials Sciences Division, Lawrence Berkeley National Laboratory, Berkeley, California 94720

M. A. Scarpulla, O. D. Dubon,
Materials Sciences Division, Lawrence Berkeley National Laboratory, and Department of Materials Sciences and Mineral Engineering, University of California, Berkeley, California 94720

J. Wu, J. Jasinski, Z. Liliental-Weber, J. W. Beeman,
Materials Sciences Division, Lawrence Berkeley National Laboratory, Berkeley, California 94720

M. R. Pillai, M. J. Aziz
Division of Engineering and Applied Sciences, Harvard University, Cambridge, MA 02138

ABSTRACT

We present a systematic investigation on the formation of the highly mismatched alloy GaN_xAs_{1-x} using N^+-implantation followed by a combination of pulsed laser melting and rapid thermal annealing. Thin films of GaN_xAs_{1-x} with x as high as 0.016 and an activation efficiency of the implanted N up to 50% have been synthesized with structural and optical properties comparable to films grown by epitaxial deposition techniques with similar substitutional N content. The effects of N^+ implantation dose, laser energy fluence and rapid thermal annealing temperature on the N incorporation as well as optical and structural properties of the GaN_xAs_{1-x} films are discussed.

PACS numbers: 71.20.Nr; 78.20.-e; 61.72.Vv; 81.40.Wx

INTRODUCTION

Recently, we have witnessed the emergence of highly mismatched semiconductor alloys (HMAs), a new class of materials whose fundamental properties are dramatically modified through the substitution of a small fraction of host atoms (less than 5 mole percent) with a very different element [1,2]. Important examples of these novel highly mismatched systems include III-N_x-V_{1-x} alloys (e.g. GaN_xAs_{1-x}) in which a small concentration (x up to ~0.05) of the highly electronegative nitrogen atom substitutes the more metallic column V element [2-13]. The most striking feature of such alloys is the large N-induced bowing of the band gap, whereby the band gap decreases by as much as 180 meV per percent of N in GaN_xAs_{1-x} [2,5].

The large band gap bowing in HMAs can be explained by an anticrossing interaction between localized states of the more electronegative element (e.g., N compared to As in GaN_xAs_{1-x}) and the extended states of the host semiconductor matrix [14,15] which splits the conduction band into two subbands. In the band anticrossing (BAC) model, the dispersion relations for the upper (E_+) and lower (E_-) conduction subbands of GaN_xAs_{1-x} are given by:

$$E_{\pm}(k)=\frac{1}{2}\left[E_N + E_M(k) \pm \sqrt{(E_N - E_M(k))^2 + 4C_{NM}^2 x} \right] \qquad (1)$$

where E_N is the energy of the N level, $E_M(k)$ is the dispersion relation for the host semiconductor matrix, and C_{NM} is the matrix element describing the coupling between N states and the extended states. For GaN_xAs_{1-x}, the downward shift of the lower subband E_- can account well for the reduction of the fundamental band gap using a value of E_N=1.65 eV above the valence band maximum derived from photoluminescence (PL) measurements in N-doped GaAs [16] and C_{NM}=2.7 eV from fitting data on the variation

of the band gap with N content [14,15]. The modification of the conduction band in other HMAs including ZnS_xSe_{1-x} ZnS_xTe_{1-x}, $ZnSe_xTe_{1-x}$ and the II-O_x-VI_{1-x} alloys is also well described by the BAC model [1,17,18].

The incorporation of these relatively small quantities of alloying species into the host semiconductor may, upon first consideration, seem as a routine challenge which can be met using today's most advanced materials synthesis techniques. However, this is far from actuality. These novel semiconductors are materials of extreme compositions that extend far beyond the thermodynamically allowed solubility and exist at the limit of kinetic stability. Thus, the epitaxial growth of highly mismatched alloys (HMAs) is still a formidable task even when using the most advanced non-equilibrium deposition processes such as molecular beam epitaxy (MBE). The formation of GaN_xAs_{1-x} thin films by N^+ implantation in GaAs followed by rapid thermal annealing (RTA) has also been explored [19-22]. With RTA an activation efficiency—defined as the ratio of substitutional N in the As sublattice to implanted N—of only ~10 to15% is achievable for implanted N mole fractions (x_{imp}) less than 0.036. The highest active N fraction x_{act} reported using RTA is $x_{act} \approx 0.004$ for $x_{imp} \approx 0.036$, corresponding to an activation efficiency of only 11% [21].

Pulsed laser melting (PLM) of ion implanted Si and GaAs was studied extensively in the late 1970s and early 1980s [23, 24]. It involves the melting of the implant-damaged or amorphized layer induced by the near surface absorption of intense (pulsed) laser radiation and the subsequent rapid epitaxial regrowth from the liquid. Epitaxy is seeded at the solid-liquid interface by the crystalline bulk in a manner very similar to liquid phase epitaxy (LPE) but with the whole process occurring on a much shorter time scale, typically between 10^{-8}-10^{-6} second. It was shown that using the PLM method amorphous layers of GaAs formed by high dose implantation could be regrown into single crystals with electrical activities of dopants well above those achievable by furnace annealing [24]. Here we report a systematic investigation on the synthesis of $Ga_{1-x}N_xAs$

layers by N^+-implanted GaAs using pulsed laser melting followed by RTA. The effects of ion dose, laser fluences and RTA temperature are addressed.

EXPERIMENT

Nitrogen ions (N^+) were implanted into semi-insulating GaAs wafers. Two N^+ implants with energies of 80 and 33keV with doses of $3.5x10^{15}$ and $1.2x10^{15}$ cm^{-2}, respectively, were used to create ~2000Å thick layers with a uniform N atomic concentration of ~$2.2x10^{20}cm^{-3}$ (1 mole percent). Layers with total implanted N contents of 2 and 4% were also formed by increasing the total N^+ dose by 2 and 4 times, respectively. All implantations were carried out using a beam current of ~0.2-0.5μA/cm^2. We emphasize that only a fraction of the implanted N (x_{imp}) becomes "active" by occupying the As sublattice (x_{act}) after annealing (i.e., $x_{act} \leq x_{imp}$).

The top of the N^+-implanted GaAs samples were pulsed-laser melted in air using an XeCl excimer laser (λ=308nm) with pulse duration ~30ns. After passing through a multi-prism homogenizer, the fluence at the sample ranged between 0.2 and 0.7J/cm^2. The melt duration (τ_{melt}) was determined by monitoring the time resolved reflectivity (TRR) of the samples using an argon-ion laser. Some of the samples were subjected to rapid thermal annealing between 600 and 950°C for 10 seconds in flowing N_2 after the PLM.

The crystalline structure of the GaN_xAs_{1-x} samples was studied by channeling Rutherford backscattering spectrometry (c-RBS) in the <100> direction. Selected samples were also investigated by cross-sectional transmission electron microscopy (xTEM). xTEM specimens were prepared by the standard method of mechanical thinning followed by ion milling. TEM studies were carried out using a TOPCON 002B microscope operated at 200 kV. The band gaps of the films were measured using photomodulated reflectance (PR) at room temperature. Radiation from a 300W halogen

tungsten lamp dispersed by a 0.5m monochromator was focused on the samples as a probe beam. A chopped HeCd laser beam (λ=442 nm or 325nm) provided the photomodulation. PR signals were detected by a Si or Ge photodiode using a phase-sensitive lock-in amplification system. The values of the band gap and the line width were determined by fitting the PR spectra to the Aspnes third-derivative functional form. [25]

RESULTS AND DISCUSSION

1. Nitrogen activation efficiency

In a previous report, we demonstrated that pulsed laser melting followed by rapid thermal annealing (PLM-RTA) greatly enhanced the incorporation of substitutional N in N^+-implanted GaAs [26]. Films implanted with 1.8% N exhibited a fundamental band gap of 1.26eV (a band gap reduction of 160meV), corresponding to an N activation efficiency of ~50%. Compared to films produced by N^+ implantation and rapid thermal annealing only, the introduction of PLM improves N incorporation by a factor of five. It was found that subsequent RTA at temperatures higher than ~700ºC after PLM was essential in obtaining good quality GaN_xAs_{1-x} thin films with clear optical transitions [26]. The optical properties and crystalline quality of these films are comparable to GaN_xAs_{1-x} thin films of similar composition made by epitaxial growth techniques.

Fig. 1 shows a series of photomodulated reflectance (PR) spectra from samples implanted with increasing amounts of N processed by PLM with energy fluence of 0.34 J/cm^2 and subsequently RTA at 950ºC for 10s. Such PLM-RTA post-implantation treatments represent the "optimum" conditions giving rise to clear, sharp optical transitions. The effects of different PLM and RTA conditions will be discussed below. PR spectra from all of the PLM-RTA samples shown in Fig. 1 exhibit distinct optical transitions across the fundamental band gap of the material. The optical transition

energies of the various samples are indicated in the figure. A monotonic decrease in the band gap with increasing implanted N content x_{imp} is clearly observed in Fig. 1, indicating an increasing fraction of N is incorporated in the As sublattice with increasing x_{imp}.

The band gaps—transitions from the valance band maximum to the lower subband E_-—of the GaN_xAs_{1-x} layers synthesized by N^+ implantation and subsequent "optimum" PLM-RTA are plotted in Fig. 2 (a) as a function of implanted N. The amount of N incorporated in the As sublattice ("active" N) for these GaN_xAs_{1-x} layers can be calculated using the band anticrossing (BAC) model for highly mismatched alloys (HMAs) expressed in Equation (1). Fig. 2 (b) shows the "active" N contents calculated using the values of E_- from Fig. 2(a) and Equation (1). The dashed line represents 100% activation, i.e. $x_{act}=x_{imp}$. Also shown is the "active" N content in GaN_xAs_{1-x} layers synthesized by N^+-implantation followed by RTA (800ºC 10s) alone from reference 21.

The results in Fig. 2(b) demonstrate that using the PLM-RTA method, the N incorporation efficiency is ~50% (slightly lower for the high dose case), over five times higher than that observed in samples synthesized by RTA alone. This can be attributed to the extremely short melt duration (~200 nsec) and regrowth process that promotes N substitution in the As subslattice and inhibits the formation of nitrogen related voids, which have recently been observed in samples formed by N^+-implantation followed by RTA only [27].

In addition to the E_- level, the BAC model also predicts an upper subband E_+ as a result of the anticrossing interaction of the localized N states and the extended conduction band states of GaAs. This electronic transition to the E_+ level has been observed in GaN_xAs_{1-x} thin films grown by epitaxial techniques for $x>0.008$ when it becomes resolvable from the spin-orbit transition ($E_0 + \Delta$) [13, 14]. The inset of Fig. 1 shows a PR spectrum taken over a wide photon energy range (1-2.2eV) from the 2% N^+-implanted GaAs followed by optimum PLM-RTA processing where $x\approx0.009$. In addition to the

fundamental band gap transition at 1.25eV, a transition at 1.8eV is observed. This high energy transition is in excellent agreement with transition to the E_+ level as calculated using Equation (1) (1.81eV). The observation of the E_+ transition further confirms the successful formation of GaN_xAs_{1-x} thin films by N^+-implantation in GaAs processed by PLM-RTA.

2. Crystalline structure of N^+-implanted GaAs layers processed by PLM and RTA

The structural damage of GaAs by N^+ implantation was studied by channeling RBS in the <100> orientation. Fig. 3 shows the c-RBS spectra from unimplanted GaAs and N^+-implanted GaAs samples with x_{imp}= 1, 2 and 4%. Notice that the <100> aligned spectra from the N^+-implanted GaAs sample do not reach the "random" (non-channeling) level. This suggests that the sample is highly damaged yet still crystalline even for the sample with x_{imp}=4%. This is consistent with the high dynamic annealing rate of GaAs at room temperature during implantation [28]. For the samples with x_{imp}=1 and 2%, dechanneling (change in slope in the c-RBS spectrum) is observed in the spectra with no observable direct scattering peak, indicating that the majority of the damage present in the top 200 nm layer of the sample consists of extended crystalline defects [29]. For the sample with x_{imp}=4%, a direct scattering peak is observed at ~150 nm below the surface. This can be attributed to the presence of either displaced Ga and As atoms or amorphous regions in the sample.

The c-RBS spectra from a N^+-implanted GaAs sample with x_{imp}=2% for the as-implanted condition, after PLM with 0.34 J/cm^2,and after PLM followed by RTA at 950ºC for 10s are shown in Fig. 4 (a). The <100> aligned spectrum from the sample exposed to a pulse fluence of 0.34J/cm^2 alone shows complete recrystallization of the implanted layer. The normalized yield χ (the ratio of channeled to random yields) in this recrystallized layer is ~0.08, slightly higher than that for perfect unimplanted GaAs

(χ=0.04). This suggests that the epitaxially regrown layer is still defective after PLM, likely containing extended crystalline defects.

Figure 4(b) shows the normalized RBS yields from 4 (a) plotted against depth below the GaAs surface. In addition the calculated N distribution [30] for the 2% N^+-implantation is also included. For the sample made by PLM alone, a high dechanneling slope is noticeable at ~0.18μm below the surface (indicated by the arrow), suggesting that the region above this point melted and epitaxially regrew from the liquid phase at this energy fluence. Since the underlying GaAs was still defective due to the end-of-range implantation damage, a high concentration of defects accumulates at the regrowth interface. Additional RTA at 950ºC for 10s removed these interfacial defects. c-RBS measurements on the PLA-RTA sample shows much improved crystalline quality, approaching that for unimplanted GaAs. The RBS results are consistent with the optical experiments that show clear optical transitions only after RTA following PLM.

The structure of the 2% N^+-implanted sample subjected to PLM-RTA was further studied by cross sectional transmission electron microscopy (xTEM). Fig. 5 shows bright-field xTEM images comparing the microstructure of a sample with x_{imp}=2% processed only by RTA with a sample treated by the PLM-RTA process (with energy fluence of 0.34J/cm^2). The RTA-only sample (Fig. 5(a)) shows a highly defective layer at depths of about 0.1-0.4 μm. In this region numerous dislocations loops are present. Many of these loops, especially the large ones, interact and form networks. A high density of nanometer-sized bubbles, which are probably filled with nitrogen gas, is also seen in this region [27]. This highly defective area is then followed by a region containing the "end-off range" defects that extends to a depth of ~0.5 μm. These are mostly extrinsic dislocations loops located on {111} planes.

In contrast to the RTA-only sample the xTEM image of the PLM-RTA sample (Fig. 5 (b)) shows that the subsurface layer is free from structural defects. Close examination of Fig. 5 (b) reveals a sharp interface at ~0.2 μm below the surface

separating two regions indicated by arrows in the figure. We believe this to be the interface between the laser-melted and then recrystallized top layer and the unmelted substrate. This interface is clearly visible in the bright-filed image taken under two beam conditions shown in Fig. 5 (c). High resolution images of this interfacial region shown in the inset of Fig. 5(c) show that there is much less crystalline disorder/clustering in the area above than in the area below this interface. However, small bubble-like defects typically less than 5nm in size are still present. We note that the "end-off range" defects remain below this interface. xTEM images on samples PLM with 0.61J/cm^2 reveals that the laser melted region extended to >0.3 μm.

3. Effects of laser energy fluence on N activation

Fig. 6 shows the normalized yield versus depth obtained from c-RBS spectra measured from a series of 2% N^+-implanted GaAs samples after PLM. The threshold energy fluence for melting GaAs was determined by TRR to be ~0.2J/cm^2. From the onset of the high dechanneling slope in the c-RBS spectra, we estimate the melt-regrown layers for samples subjected to 0.24 and 0.34J/cm^2 laser pulses to be ~0.12 and 0.18μm, respectively. For energy fluences >0.47J/cm^2, the dechanneling slope in the c-RBS spectra is no longer observable, indicating that the laser-melted layer exceeds the regions with significant amounts of implant-damage (>0.25μm). These ion channeling results are in good agreement with the xTEM measurements mentioned previously.

PR spectra from the samples shown in Fig. 6 with additional RTA at 950ºC for 10s are shown in Fig. 7. The fundamental band gap transition at 1.25eV is not affected by the laser energy fluence. This suggests that increasing the energy fluence does not influence the N incorporation in the film. Similar results on the lack of energy fluence dependence on N incorporation are also observed for the sample with x_{imp}=1% N. Since the melt depth exceeds the implanted GaAs layer thickness for the high laser energy fluence, one might expect a decrease in the N incorporation if the N atoms are free to re-

distribute in the melted layer to form N_2 molecules. The fact that the incorporation of N atoms does not depend on energy fluence suggests that they do not diffuse significantly in the short melt duration of hundreds of nanoseconds.

In the PR spectrum from the sample exposed to an energy fluence of 0.24J/cm^2, another prominent feature is observed at around 1.4eV. Since the N^+-implanted GaAs region is ~0.2μm thick and the laser-melted region is estimated from c-RBS to be only ~0.1μm for this energy fluence, the underlying N-containing layer is expected to be similar to samples subjected to RTA only. Indeed, the broad line shape and the position of this transition are similar to those from a GaN_xAs_{1-x} layer formed by RTA alone [21]. In addition to the increase in melting depth as measured by c-RBS and TEM, raising the energy fluence also results in an increase in the melt duration τ_{melt}, which was measured to be ~100-300 nsec for the energy fluence range of 0.24-0.61J/cm^2.

The effect of laser energy fluence on the band gap (as determined from PR spectra) and on N incorporation in GaAs samples with x_{imp}=1, 2 and 4% is displayed in Fig. 8 (a) and (b), respectively. While the band gap and thus the N incorporation is not dependent on the energy fluence for the samples with x_{imp}=1 and 2%, the band gap of the samples with x_{imp}= 4% followed by PLM and RTA depends strongly on the energy fluence of the laser pulse. Increasing the energy fluence in this case results in an increase in the band gap and a decrease in the amount of incorporated N. At a fluence of 0.61J/cm^2, a similar amount of incorporated N (~0.8%) is found for both the 2 and 4% N-implanted samples. This can be attributed to the high N content in the GaAs that exceeds the kinetic limit of solubility even for the short melt duration of ~300nsec. Hence the longer duration of the melt associated with the higher fluence enables the N atoms to migrate to the surface or to coalesce and form bubbles (i.e., N-related voids). This may account for the reduced N activation in these high x_{imp} samples as the energy fluence increases.

4. Effects of RTA temperature

As mentioned above, distinct optical transitions in N^+-implanted GaAs are observable only after PLM and RTA at temperatures higher than 700ºC. This is consistent with the c-RBS measurements on the PLM samples that showed the presence of structural defects after the PLM process. Fig. 9 shows a series of representative PR spectra from N^+-implanted GaAs samples with x_{imp}=2% after PLM at a fluence of 0.34J/cm^2 followed by RTA for 10 seconds in the temperature range of 600-950ºC. Only a very weak and vague optical transition is observed for the sample processed only by PLM due to the high concentration of defects that remains in the regrown layer. The optical transition attributable to the band gap at ~1.2-1.3eV becomes very clear after RTA at 700ºC. The linewidth of this transition continues to narrow as the RTA temperature increases, indicating the improvement in the crystallinity of the layer.

The inset of Fig. 9 shows the band gap and the linewidth of the optical transitions measured by PR as a function of the RTA temperature. A slight, gradual increase in the band gap with increasing RTA temperature is observed. For RTA at 950ºC, the band gap increases by 20meV with respect to the sample not treated by RTA. This change in the band gap, although observable, accounts to only ~12% of the total band gap reduction and corresponds to a reduction in active N incorporated in the layer from x_{act}=0.0107 to 0.0093.

As a comparison, for N^+-implanted GaAs samples subjected to RTA only, annealing above 870ºC resulted in less than 0.1%N incorporation in GaAs [21]. We believe that this is due to the presence of a high concentration of vacancies in the N-implanted samples. Upon RTA these vacancies recombine and also act as sinks for the N atoms, promoting the clustering of N into voids. A recent transmission electron microscopy investigation revealed that in the N^+-implanted GaAs sample after RTA at 950°C a very high density of N-related small voids, with an average size of about 2-3 nm is present in the implanted layer [27]. In the case of PLM the process of rapid melting

and solidification may result in the annihilation of implantation-induced vacancies as well as a complete local rearrangement of the atom sites leading to the formation of strong Ga-N bonds, thus stabilizing N atoms on the anion sites. The subsequent, lower temperature RTA cannot break these bonds but can improve the overall crystal quality by short range atomic diffusion and rearrangement. In MOCVD grown GaN_xAs_{1-x} layers, N atoms on As sites are also found to be thermally stable at RTA at 950ºC.

A narrowing of the linewidth of optical transitions observed in PR measurement occurs as the RTA temperature is increased. This is depicted in the inset of Fig. 9. Increasing the RTA temperature results in the more effective removal of structural imperfections present after PLM processing. The improved crystal quality of the implanted layer leads to sharper optical transitions. For samples synthesized by PLM and RTA at 950ºC, the linewidth of the optical transition becomes comparable to that from GaN_xAs_{1-x} thin films with similar N composition that were epitaxially grown by metalorganic chemical vapor deposition (<30 meV) [13].

CONCLUSION

In conclusion we have carried out a systematic investigation on the formation of the highly mismatched alloy GaN_xAs_{1-x} using N^+ implantation followed by a combination of pulsed laser melting and rapid thermal annealing. With an optimized treatments on a GaAs substrate implanted with 4% N^+, GaN_xAs_{1-x} thin films with x as high as 0.016 have been synthesized. For implanted N concentrations below 4%, a N activation efficiency as high as 50% can be achieved. Increasing the energy fluence of the pulsed laser above the threshold (~0.2J/cm^2) increases both the melt duration and melt depth. We found that energy fluence does not alter the N incorporation for concentrations of implanted N below 2%. For samples implanted with 4% N, increasing the PLM energy fluence dramatically reduces the N incorporation to a value close to that observed for samples

implanted with N to a level of 2%. As the RTA temperature is increased, a gradual decrease in the linewidth of the PR transition and a slight increase in the band gap are noticed. This indicates that the RTA process following PLM improve the crystallinity of the layers with little N deactivation.

ACKNOWLEDGMENTS

This work is supported by the Director, Office of Science, Office of Basic Energy Science, Division of Materials Sciences and Engineering, of the U.S. Department of Energy under Contract No. DE-AC03-76SF00098. MAS acknowledges support from an NSF graduate research fellowship. The work at Harvard was supported by NASA grant # NAG8-1680.

REFERENCES

1. W. Walukiewicz, W. Shan, K. M. Yu, J. W. Ager III, E. E. Haller, I. Miotlowski, M. J. Seong, H. Alawadhi, and A. K. Ramdas, *Phys. Rev. Lett*. **85**, 1552 (2000).
2. see for example, Semiconductor Science and Technology **17**, 2002, Special Issue: III-N-V Semiconductor Alloys.
3. S. Sakai, Y. Ueta and Y. Terauchi, *Jpn. J. Appl. Phys*. **32**, 4413 (1993).
4. M. Kondow, K. Uomi, K. Hosomi, and T. Mozume, *Jpn. J. Appl. Phys.* **33**, L1056 (1994).
5. K. Uesugi, N. Morooka, and I. Suemune, *Appl. Phys. Lett. **74***, 1254(1999).
6. J. F. Geisz, D. J. Friedman, J. M Olson, S. R. Kurtz, and B. M. Keyes, *J. Cryst. Growth* **195**, 401 (1998).
7. M. Kondow, T. Kitatani, M. C. Larson, K. Nakahara, K. Uomi and H. Inoue, *J. Crystal Growth* **188**, 255 (1998).
8. D. J. Friedman, J. F. Geisz, S. R. Kurtz, D. Myers and J. M Olson, *J. Cryst. Growth* **195**, 409(1998).
9. S. R. Kurtz, A.A. Allerman, E.D. Jones, J.M. Gee, J.J. Banas, and B.E. Hammons, *Appl. Phys. Lett*. **74**, 729(1999).
10. J. N. Baillargeon, K. Y. Cheng, G. E. Hofler, P. J. Pearah and K. C. Hsieh, *Appl. Phys. Lett.* **60**, 2540 (1992).
11. W. Shan, W. Walukiewicz, K. M. Yu, J. Wu, J. W. Ager, E. E. Haller, H. P. Xin, and C. W. Tu, *Appl. Phys. Lett*. **76**, 3251 (2000).
12. W. G. Bi and C. W. Tu, *J. Appl. Phys*. **80**, 1934 (1996).
13. W. Shan, W. Walukiewicz, K. M. Yu, J. W. Ager III, E. E. Haller, J. F. Geisz, D. J. Friedman, J. M. Olson, Sarah R. Kurtz, and K. Nauka,Phys. Rev. **B62**, 4211 (2000).
14. W. Shan, W. Walukiewicz, J. W. Ager III, E. E. Haller, J. F. Geisz, D. J. Friedman, J. M. Olson, and S. R. Kurtz, *Phys. Rev. Lett.* **8**2, 1221(1999).

15. J. Wu, W. Shan, and W. Walukiewicz, Semicond. Sci. Technol. **17**, 860 (2002).

16. D. J. Wolford, J. A. Bradley, K. Fry, and J. Thompson, in *Proceedings of the 17th International Conference on the Physics of Semiconductors*, edited by J. D. Chadi and W. A. Harrison (Springer, New York, 1984) p. 627.

17. K. M. Yu, W. Walukiewicz, J. Wu, J. W. Beeman, J. W. Ager, E. E. Haller, I. Miotkowski, A. K. Ramdas, and P. Becla, Appl. Phys. Lett. **80**, 1571 (2002).

18. Kin Man Yu, J Wu, W. Walukiewicz, J. W. Beeman, J. W. Ager, E. E. Haller, I. Miotkowski, and A. Ramdas, J. Electron. Mater. **31**, 754 (2002).

19. W. Shan, K. M. Yu, W. Walukiewicz, J. W. Ager, E. E. Haller and M. C. Ridgway, *Appl. Phys. Lett*. **75**, 1410 (1999).

20. K. M. Yu, W. Walukiewicz, W. Shan, J. Wu, J. Beeman, J. W. Ager III, E. E. Haller, and M. C. Ridgway, Mater. Res. Soc. Symp. Proc. **647**, O13.3.1/R8.3.1 (2001).

21. K. M. Yu, W. Walukiewicz, J. Wu, J. W. Beeman, J. W. Ager III, E. E. Haller, W. Shan, H. P. Xin, C. W. Tu, and M. C. Ridgway, J. Appl. Phys. **90**, 2227 (2001).

22. K. M. Yu, Semicond. Sci. Tedchnol. **17**, 785 (2002).

23. C. W. White and P. S. Peercy, eds., *Laser and Electron Beam Processing of Materials* (Academic Press, New York, 1980).

24. J. S. Williams in *Laser Annealing of Semiconductors*, J. M. Poate and J. W. Mayer, eds., p. 385 (Academic Press, New York, 1982).

25. D. E. Aspnes, *Surf. Sci.* **37**, 418 (1973).

26. K. M. Yu, W. Walukiewicz, J. W. Beeman, M. A. Scarpulla, O. Dubon, M. R. Pillai, and M. Aziz, Appl. Phys. Lett. **80**, 3958 (2002)

27. J. Jasinski, K. M. Yu, W. Walukiewicz, Z. Liliental-Weber and J. Washburn, Appl. Phys. Lett. **79**, 931 (2001).

28. R. A. Brown and J. S. Williams, J. Appl. Phys. **81**, 7681 (1997).

29. L. C. Feldman, J. W. Mayer, and S. T. Picraux, *Materials Analysis by Ion Channeling* (Academic, New York, 1982).

30. PROFILE, Ion Beam Profile Code version 3.20, Implant Sciences Corp. 107 Audubon Rd., #5, Wakefield, MA 01880.

FIGURE CAPTIONS

Fig. 1 Photomodulated reflectance (PR) spectra measured from a series of samples implanted with increasing levels of N (x_{imp}) and processed by PLM at an energy fluence of 0.34J/cm^2 and subsequent RTA at 950ºC for 10 sec. The inset shows a PR spectrum from GaAs sample with x_{imp}=2% taken over a wide photon energy range (1-2.2eV) showing both the E_- and E_+ transitions.

Fig. 2 (a) Band gap energies determined from the PR spectra shown in Fig. 1. (b) Active N content estimated using the band anticrossing model and the values of E_- determined from the PR spectra in (a). The dashed line in (b) represents 100% activation for the implanted N. Also shown in (b) is the active N content in GaN_xAs_{1-x} layers synthesized by N^+-implantation followed by RTA (800ºC for 10 sec.) alone.

Fig. 3 Channeling Rutherford backscattering (c-RBS) spectra from N^+-implanted GaAs samples with x_{imp}=1, 2 and 4% taken in the <100> axial direction. The <100> aligned and random spectra from an unimplanted GaAs sample are also shown.

Fig. 4 (a) c-RBS spectra from N^+-implanted GaAs samples with x_{imp}=2% in the as-implanted condition, after PLM at an energy fluence of 0.34J/cm^2, and after PLM followed by RTA at 950ºC for 10 sec. (b) The normalized yields (ratio of the channeled to random yields) of the c-RBS data from (a) are plotted against depth below the GaAs surface. The calculated N distribution is also shown in the figure.

Fig. 5 Bright-field symmetrical cross-sectional TEM images of N^+-implanted GaAs samples with x_{imp}=2% for the following process conditions: (a) RTA at 950ºC for 10s only and (b) PLM at an energy fluence of 0.34J/cm^2 followed by RTA at 950ºC for 10sec. (c) Bright-field two-beam cross-sectional TEM image of the sample shown in (b). The inset of (c) shows a high resolution image of the

interface region. Note the much higher disorder/clustering in the area below the interface.

Fig. 6 Normalized yield as a function of depth obtained from c-RBS spectra from a series of N^+-implanted GaAs samples with x_{imp}=2% after PLM at an energy fluence in the range of 0.24-0.61J/cm^2.

Fig. 7 PR spectra from the samples shown in Fig. 5 with additional RTA at 950ºC for 10s.

Fig. 8 Band gap energy and active N concentration (x_{act}) determined from PR spectra as a function of PLM energy fluence. The samples were annealed at 950ºC for 10sec. following the PLM process.

Fig. 9 A series of representative PR spectra from N^+-implanted GaAs samples with x_{imp}=2% after PLM at an energy fluence of 0.34J/cm^2 followed by RTA for 10 sec. in the temperature range of 600-950ºC. The band gaps measured by PR and the linewidth of the optical transitions are plotted as a function of the RTA temperature (inset).

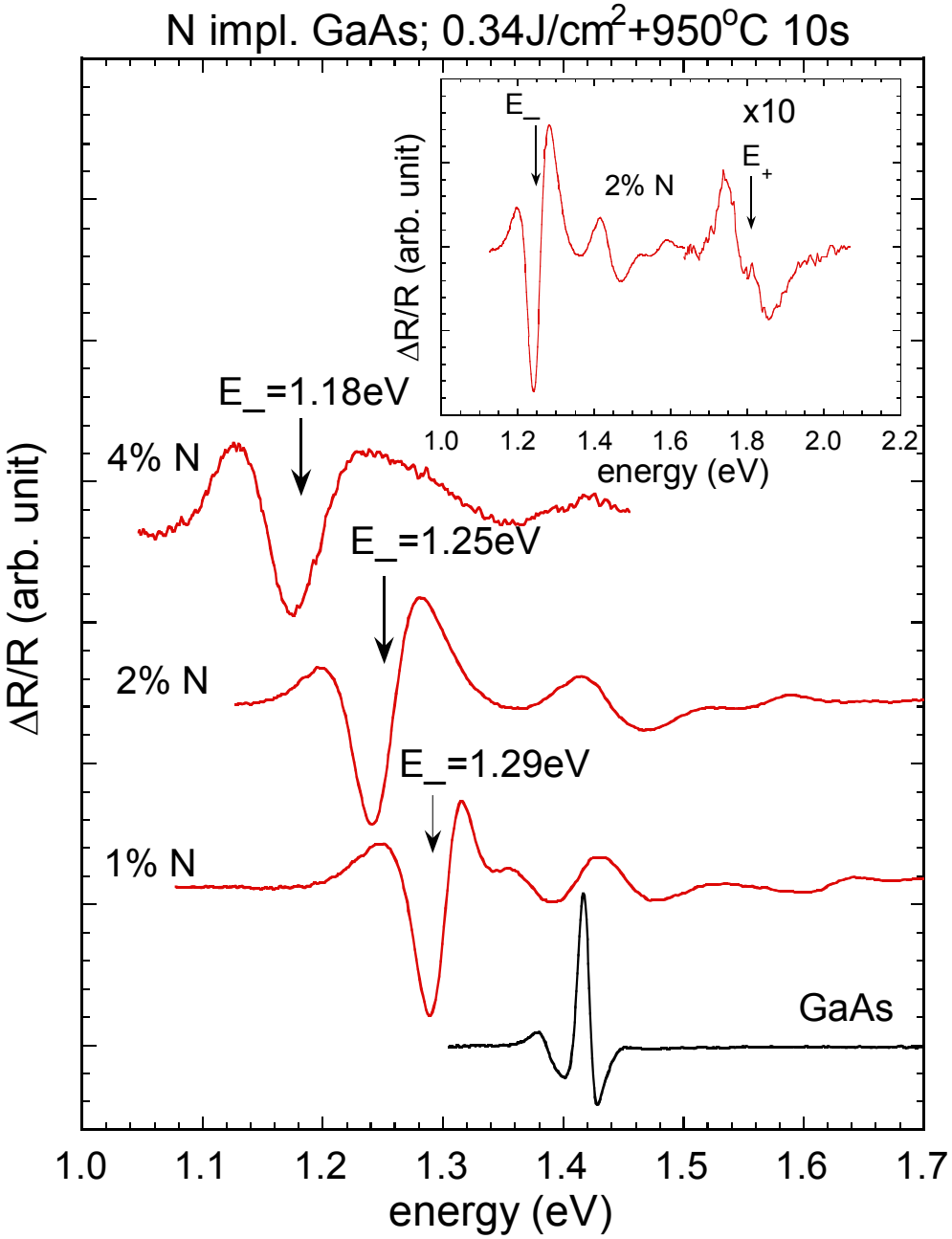
N impl. GaAs; 0.34J/cm2+950oC 10s
ΔR/R (arb. unit)
E_=1.18eV
4% N
E_=1.25eV
2% N
E_=1.29eV
1% N
GaAs
1.0
1.1
1.2
1.3
1.4
1.5
1.6
1.7
energy (eV)
E_
x10
E+
2% N
ΔR/R (arb. unit)
1.0
1.2
1.4
1.6
1.8
2.0
2.2
energy (eV)

Fig. 1

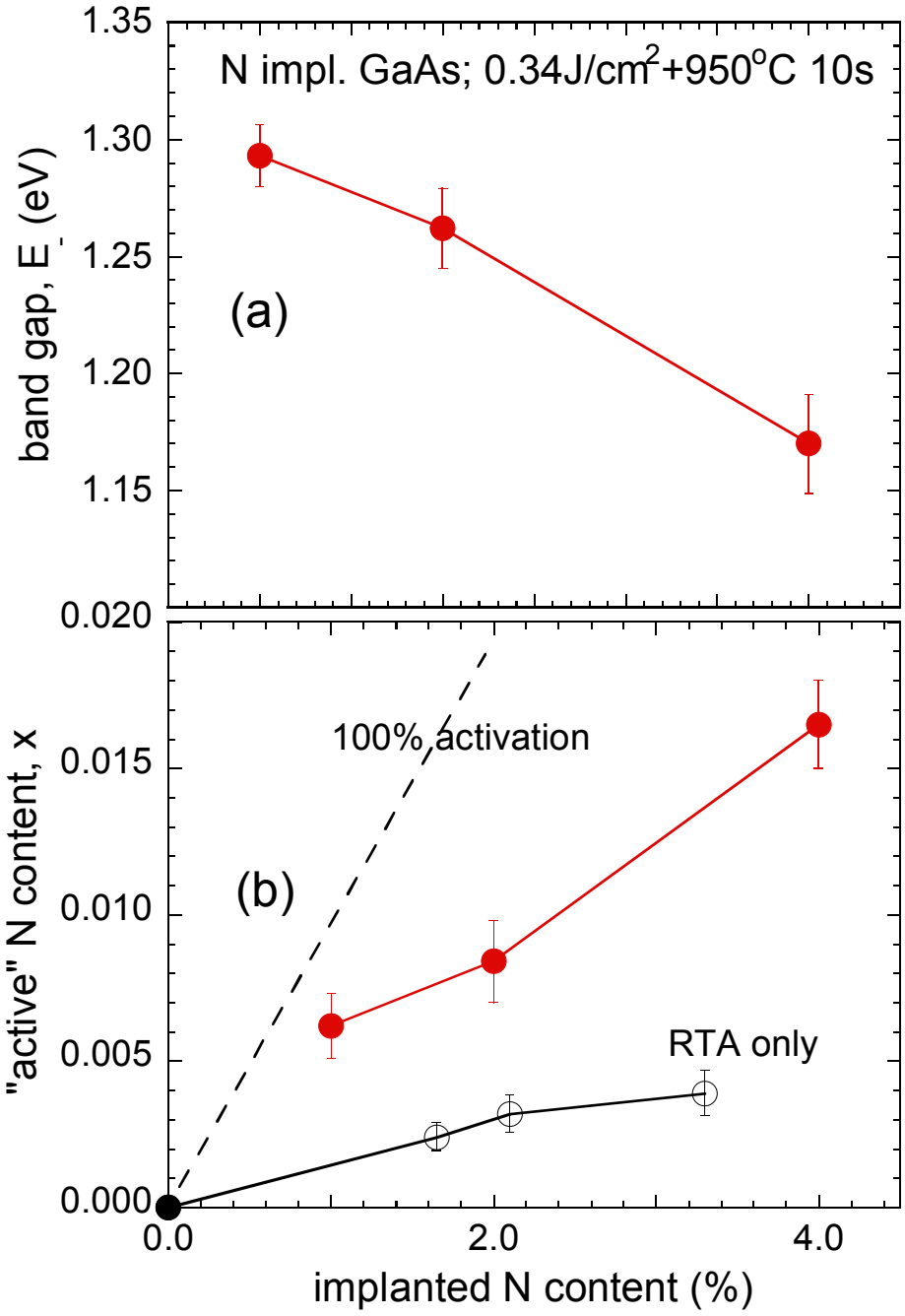
N impl. GaAs; 0.34J/cm2+950oC 10s
band gap, E- (eV)
1.35
1.30
1.25
1.20
1.15
(a)
0.020
"active" N content, x
0.015
0.010
0.005
0.000
100% activation
(b)
RTA only
0.0
2.0
4.0
implanted N content (%)

Fig. 2

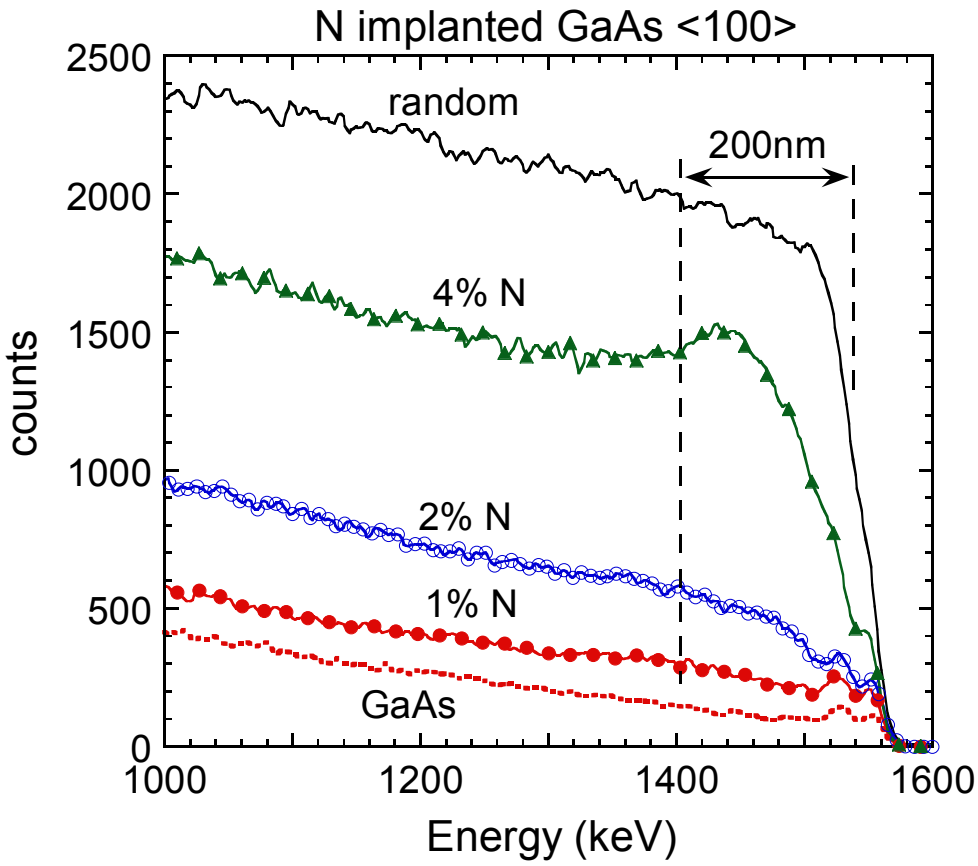
N implanted GaAs <100>
random
200nm
4% N
2% N
1% N
GaAs
counts
Energy (keV)
2500
2000
1500
1000
500
0
1000
1200
1400
1600

Fig. 3

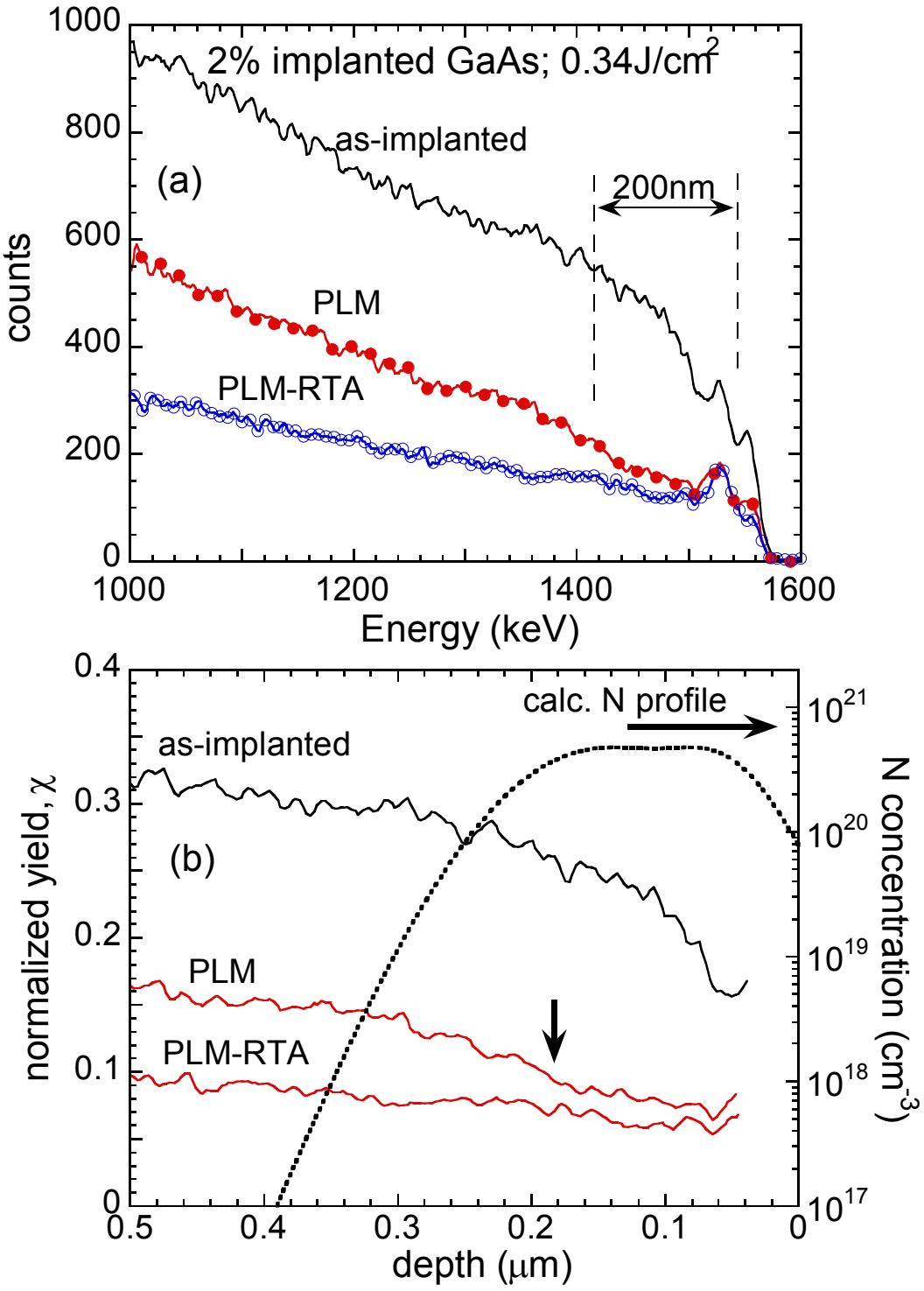
2% implanted GaAs; 0.34J/cm2
as-implanted
(a)
200nm
PLM
PLM-RTA
counts
Energy (keV)
calc. N profile
as-implanted
(b)
PLM
PLM-RTA
normalized yield, χ
N concentration (cm-3)
depth (μm)

Fig. 4

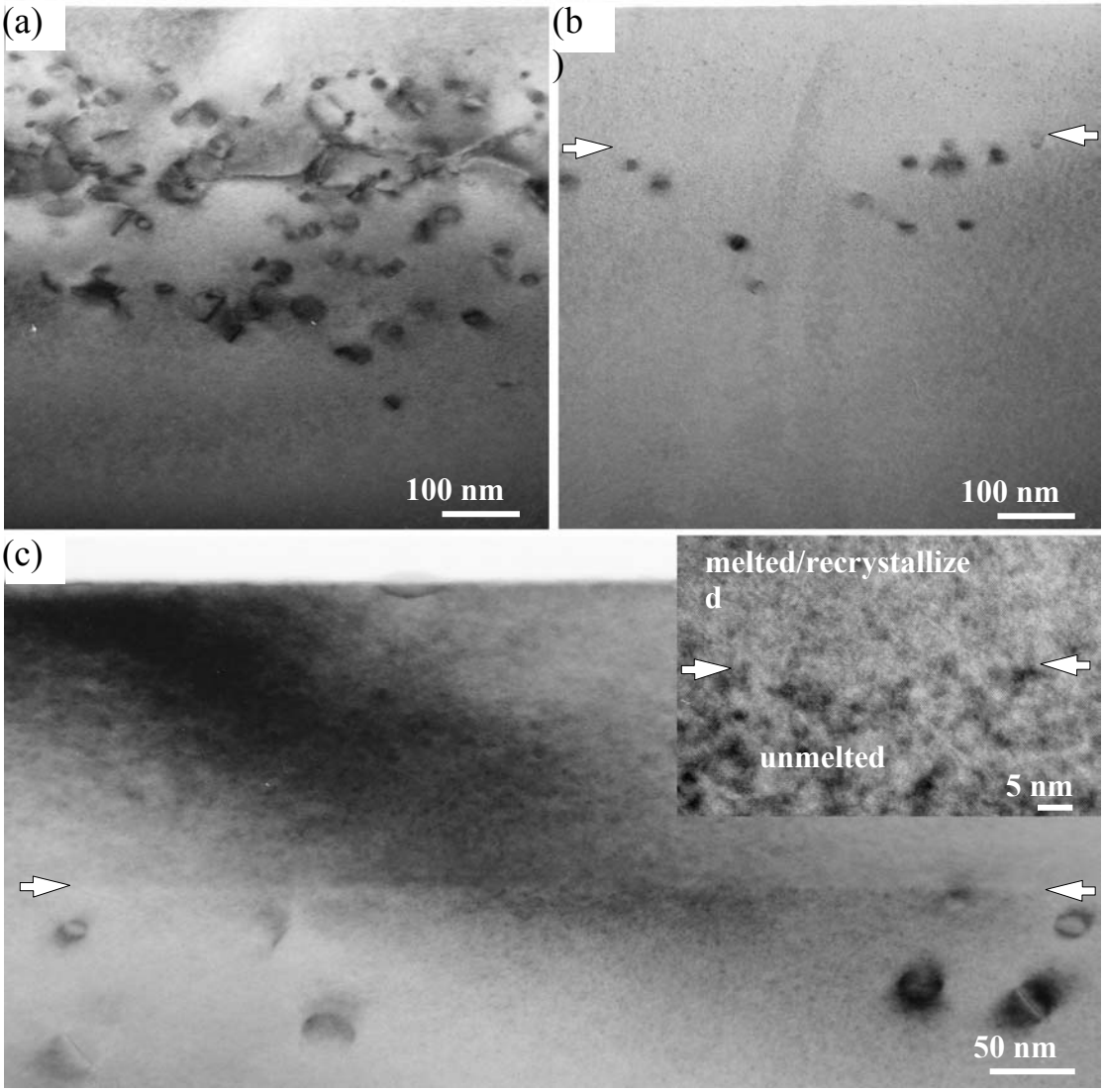

Fig. 5

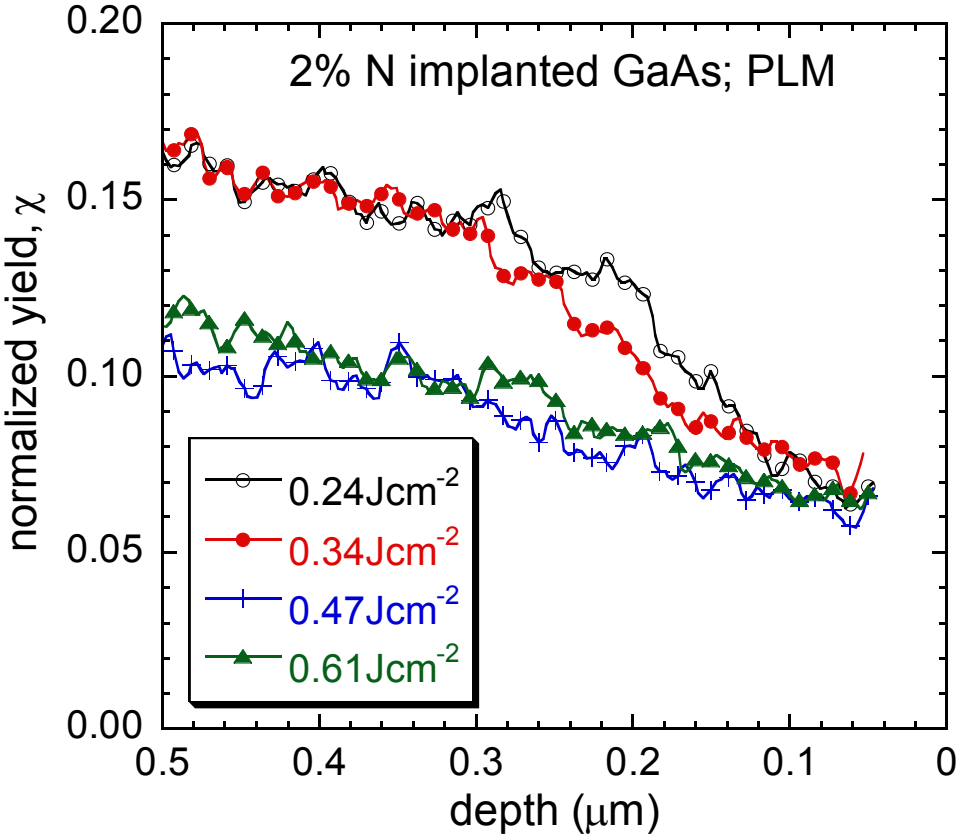
2% N implanted GaAs; PLM
normalized yield, χ
depth (μm)
0.24Jcm-2
0.34Jcm-2
0.47Jcm-2
0.61Jcm-2
0.20
0.15
0.10
0.05
0.00
0.5
0.4
0.3
0.2
0.1
0

Fig. 6

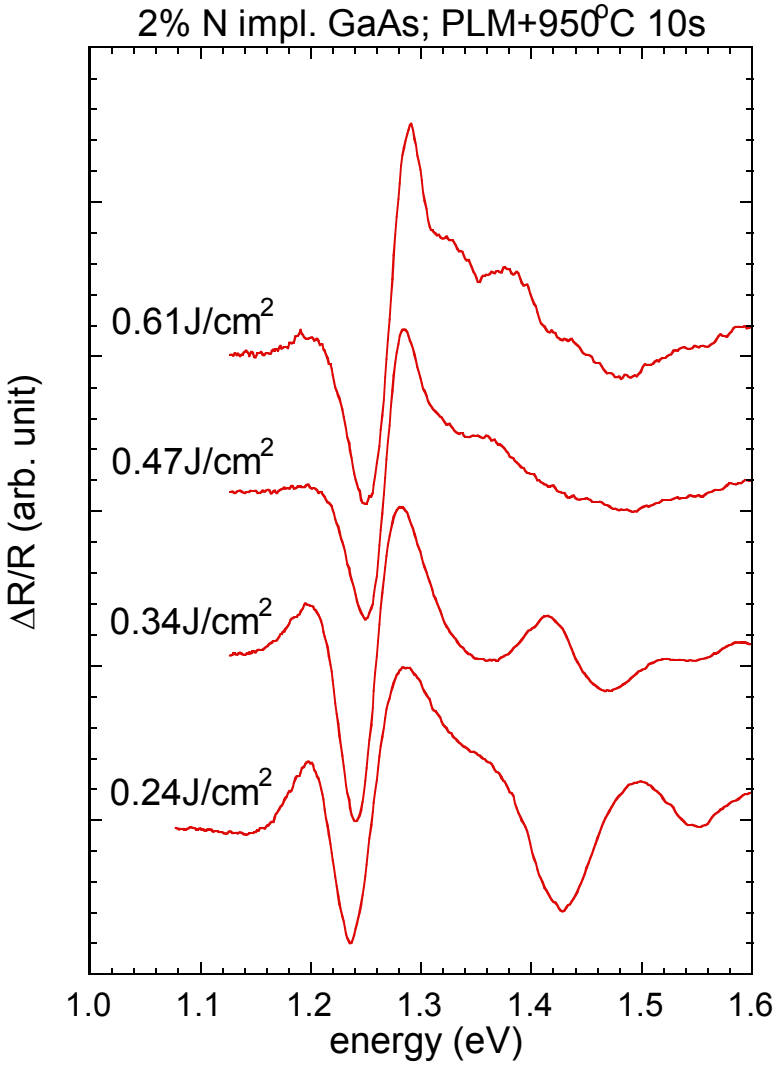
2% N impl. GaAs; PLM+950°C 10s
0.61J/cm2
0.47J/cm2
0.34J/cm2
0.24J/cm2
ΔR/R (arb. unit)
1.0
1.1
1.2
1.3
1.4
1.5
1.6
energy (eV)

Fig. 7

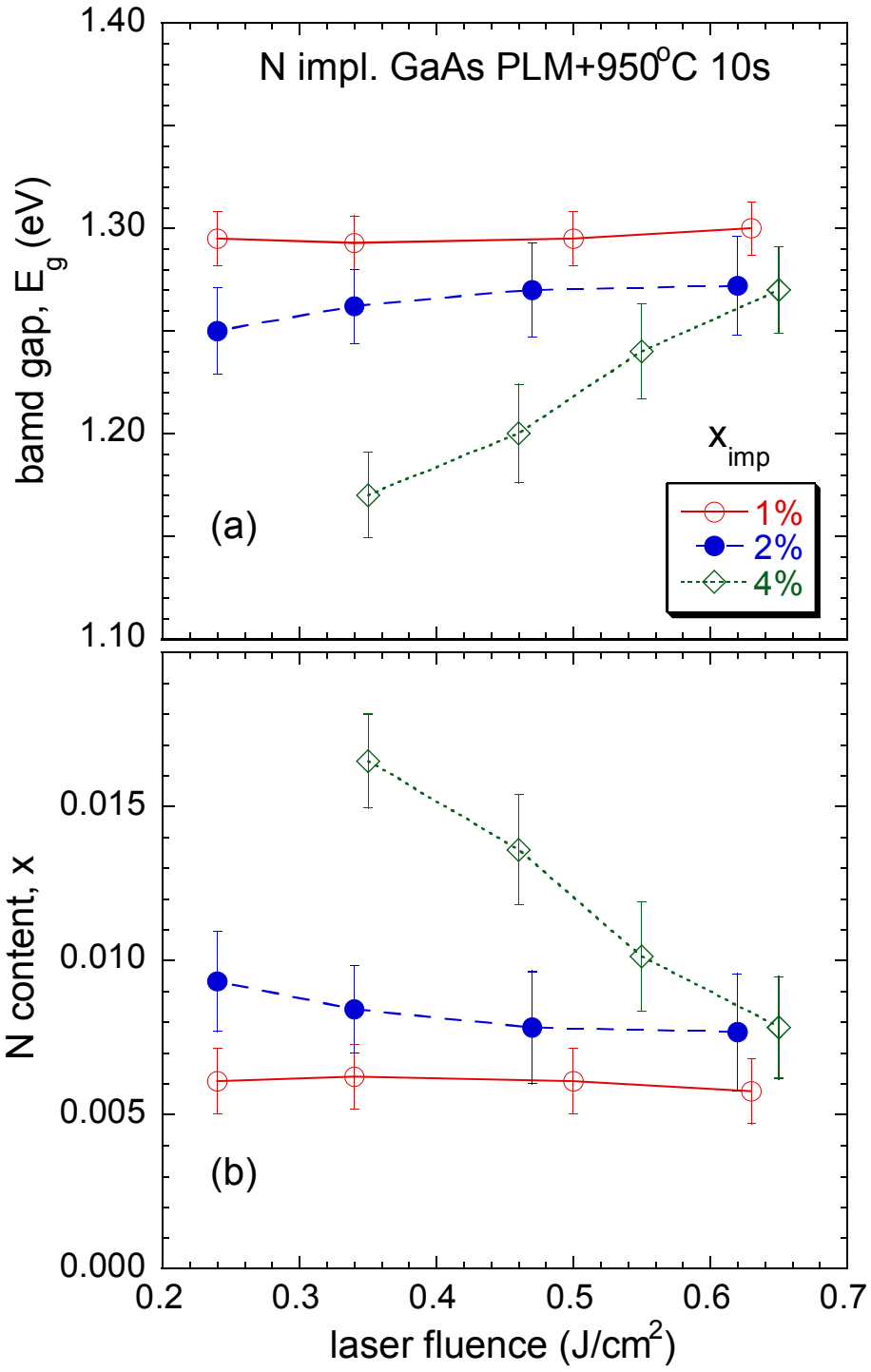
N impl. GaAs PLM+950°C 10s
bamd gap, E_g (eV)
1.40
1.30
1.20
1.10
(a)
x_{imp}
1%
2%
4%
N content, x
0.015
0.010
0.005
0.000
(b)
0.2
0.3
0.4
0.5
0.6
0.7
laser fluence (J/cm^2)

Fig. 8

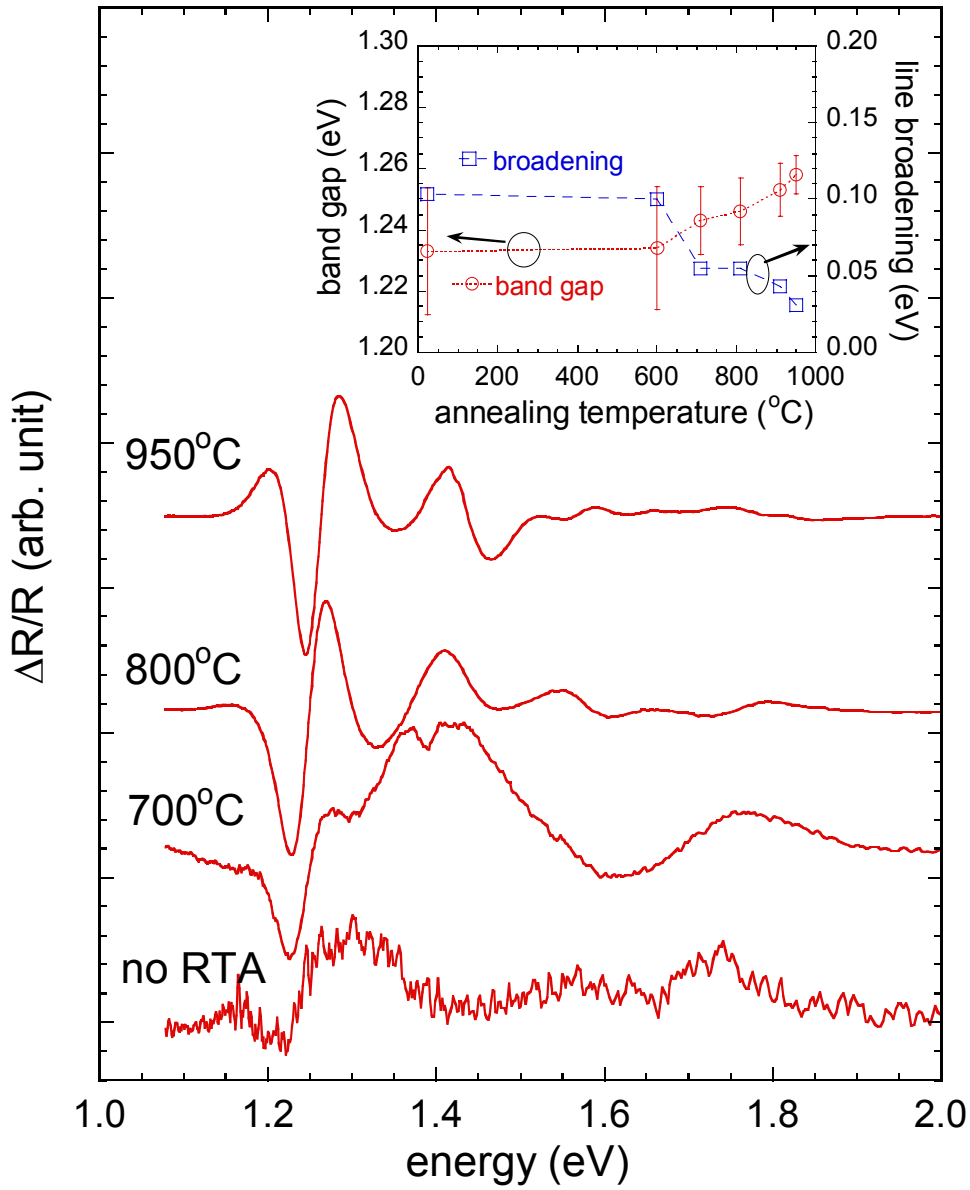
ΔR/R (arb. unit)
950°C
800°C
700°C
no RTA
1.0
1.2
1.4
1.6
1.8
2.0
energy (eV)
band gap (eV)
line broadening (eV)
broadening
band gap
1.30
1.28
1.26
1.24
1.22
1.20
0.20
0.15
0.10
0.05
0.00
0
200
400
600
800
1000
annealing temperature (°C)

Fig. 9